Turkish Journal of Physics

http://journals.tubitak.gov.tr/physics/

Research Article

Turk J Phys
(2020) 44: 77 – 84
© TÜBİTAK
doi:10.3906/fiz-1910-15

Anisotropic magnetoresistance and planar Hall effect in magnetoresistive NiFe/Pt thin film

Erdem DEMİRCİ*
Department of Physics, Faculty of Science, Gebze Technical University, Kocaeli, Turkey

Received: 16.10.2019 • **Accepted/Published Online:** 28.01.2020 • **Final Version:** 12.02.2020

Abstract: The magnetoresistive NiFe/Pt sensor was fabricated by using standard microlithography and sputter deposition techniques and then the magnetic and magnetotransport properties were investigated. The magnetic properties of the sample show that the easy axis of magnetization prefers a predefined direction along the Hall bar. Moreover, the sample has uniaxial magnetic anisotropy due to the growth-induced magnetic anisotropy. On the other hand, the Anisotropic magnetoresistance (AMR) and the Planar Hall effect (PHE) of the sample were investigated in detail between 0°and 360°. The angle-dependent AMR and PHE signals at the in-plane magnetic field of constant magnitude intersect at certain angles. At these angles, the presence of unusual peaks and valleys was observed. This is proof that AMR and PHE curves had strongly affected each other at certain angles.

Key words: Magnetoresistive sensor, planar Hall effect, anisotropic magnetoresistance, NiFe

1. Introduction

In recent years, the magnetoresistive sensors based on anisotropic magnetoresistive (AMR) have attracted great attention owing to their high sensitivity at weak magnetic fields, the flexibility of the design, and compatibility with standard microelectronics technology [1–5]. The magnetoresistive sensors are commonly used for magnetic bead detection [6], biosensors and biochips [7, 8], applications to microcompass [9], and flexible magnetic sensors [10, 11]. The physical phenomenon of the magnetoresistance effect is related to the change in the resistance of the magnetic conductor under external magnetic field [12]. The change in the resistance (R) is experimentally expressed as

$$R=R_0+\Delta R\cos^2\theta \tag{1}$$

Here, R_0 is the electrical resistance in the absence of a magnetic field, ΔR is the difference in the resistance of the magnetic conductor and θ is the angle between the current (I) and magnetization (M).

It is known that the AMR effect arises from the anisotropic scattering of conductive electrons in a ferromagnetic material [13]. In this phenomenon, the resistance is at the maximum when M and I are parallel ($R_{//}$) or it is at minimum when M and I are perpendicular with each other ($R_{\perp}$). The AMR effect with in-plane magnetization is described by Eq. (2) [13]. However, unlike the AMR in longitudinal geometry, the magnetoresistance measurement in transverse geometry causes the electric field perpendicular to the current. The phenomenon in transverse geometry is called the planar Hall effect (PHE) and it is expressed by Eq. (3) [13]. Although the PHE output voltage is very low compared to the AMR output voltage, the planar Hall effect

*Correspondence: e.demirci@gtu.edu.tr

This work is licensed under a Creative Commons Attribution 4.0 International License.

is considerably reduced the temperature drift and increased the resolution of magnetoresistive sensors [14]. For a single domain ferromagnetic conductor, electric fields (E) of AMR and PHE are expressed as follows:

$$E_{AMR}=\mathrm{j}\rho_{\perp}+\mathrm{j}(\rho_{||}-\rho_{\perp})\cos^2\theta \tag{2}$$

$$E_{PHE}=\mathrm{j}(\rho_{||}-\rho_{\perp})\sin\theta\cos\theta \tag{3}$$

Here, $\rho_{//}$ and $\rho_{\perp}$ are the resistivities for the current parallel and perpendicular to the magnetization orientations, respectively. According to Eq. 3, PHE voltage is proportional to the *sin2θ* angle between M and I. Therefore, PHE voltage is extremely sensitive rather than AMR voltage to detect small deviations in the magnetization from the current direction [15, 16]. Also, the background signals existing in the AMR are not observed in the PHE. By considering these disadvantages of AMR compared to PHE, the magnetoresistive sensor based on AMR requires high sensibility to the deviation of magnetoresistance for novel technology.

In the present work, the magnetoresistive Py (10 nm)/Pt (5 nm) sensor was fabricated with Hall bar and continuous film structures on SiO_2/Si. Then, AMR and PHE measurements of the sensor were performed in an applied external magnetic field at a different angle to compare the effect of their signal responses on each other. To observe a small deviation of magnetoresistance based on current was examined in detail by using PHE and AMR techniques.

2. Experiment and discussion

2.1. Fabrication

The magnetoresistive sensor based on AMR was designed and fabricated using standard microlithography and sputter deposition techniques. First, Hall bar and continuous patterns were realized on SiO_2/Si substrates by optical lithography. Before the lithography processes, the SiO_2/Si substrate was cleaned by sequentially rinsing in acetone, isopropanol, and deionized water. After that, a positive photoresist (AZ 1505) was coated onto the cleaned SiO_2/Si substrate by using a spin coater. To form a uniform photoresist with a thickness of 500 μm, coating processes were carried out at 4000 rpm for 50 s. The photoresist was baked on the hot plate at 110 °C for 60 s. Then, it was exposed at constant intensity ultraviolet light (365 nm, i-line) for 0.5 s and developed by using AZ 726 MIF for 60 s. After the patterning process, Py (10 nm)/ Pt (5 nm) layers were deposited on SiO_2/Si by using magnetron sputtering. Py and Pt layers were deposited at room temperature by using 20 W (RF) and 10 W (DC) powers, respectively. The base pressure level of the sputter chamber was 6 $\times 10^{-9}$ mbar and the working pressure was kept at 5 $\times 10^{-3}$ mbar during the deposition. After that, the sample was soaked in acetone for 10 min and residual photoresist on SiO_2/Si substrate was lifted off. The microscope image of the sample consists of Hall bar and continuous parts are as shown in Figure 1.

Figure 2 shows the measurement geometry for the magnetotransport experiments. In this geometry, the easy axis of the sample is parallel to I. Here, θ is the angle between I and the M, and θ_H is the angle between I and the external magnetic field (H_{ext}). Magnetoresistive experiments were performed by using a magnetotransport system. A typical current strength was supplied by a Keithley 2400 source meter and the current was fixed at 50 µA for all magnetoresistive experiments. The magnetic field-dependent voltage was measured by a Keithley 2182 nano voltmeter. The angle-dependent magnetoresistive experiments were carried out between 0°and 360°by using an integrated stepper motor. During the magnetoresistive experiments, a constant current was passed through the long direction of the Hal bar between 1 and 6 terminals for all

magnetotransport measurements. Then, the AMR voltage between 3 and 4 terminals (V_{3-4}) and PHE voltage between 2 and 3 terminals (V_{2-3}) were recorded by using nanovolt meter while the in-plane magnetic field was swept. The distance is 200 µm between the magnetoresistance terminals (V_{3-4}), and 25 µm between the planar Hall terminals (V_{2-3}). The long axis of the sample in the Hall bar is prepared with 8:1 aspect ratio to induce shape anisotropy.

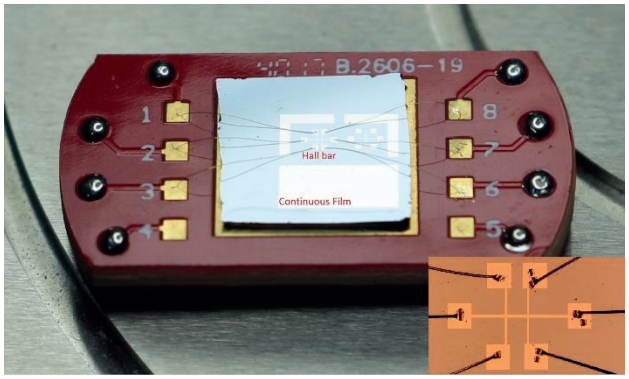

Figure 1. Photograph of the sample mounted on a printed circuit board (PCB). The sample consists of Hall bar (top) and continuous film (bottom). The contact pads and PCB terminals were connected with gold wires by using wire bonder. The inset is a microscope top-view image of the magnetoresistive Py/Pt sensor.

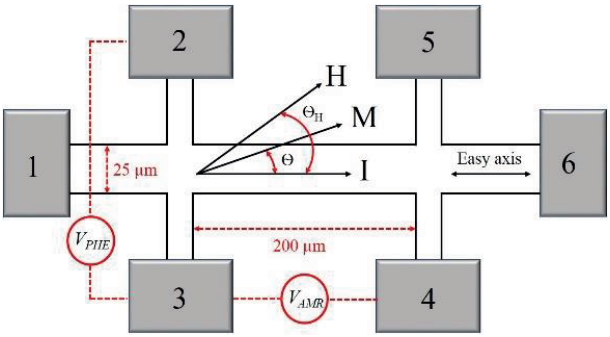

Figure 2. Schematic representation of the Hall bar geometry with the 6 terminals. The width of the Hall bar is 25 µm and the length is 200 µm. A constant current of 50 µA was passed through 1–6 terminals by using Keithley 2400 source meter. The voltage is measured 2–3 terminals for PHE and 4–5 terminals for AMR by using Keithley 2182 nanovoltmeter.

3. Results and discussion

Magnetic hysteresis loops of the sample were measured by using a magneto-optical Kerr effect (MOKE) at room temperature. First, angle-dependent longitudinal MOKE (L-MOKE) measurements were carried out from 0°to 360°by using a stepper motor. L-MOKE hysteresis loops of the Si/ SiO_2 / Py/ Pt were used for the determination of the angular dependence of the normalized remanent magnetization (M_R/M_S) as shown in Figure 3. The sample exhibits in-plane uniaxial magnetic anisotropy. The growth-induced anisotropy is the major cause of this behavior of the sample since direction of magnetization is closely related to the growth conditions in the magnetron sputtering systems. During deposition, the substrate is deposited with atoms from an oblique angle; thus, magnetization can be oriented in a specific direction. Here, the easy axis of the magnetization prefers to extend along the Hall bar of the sample due to the growth-induced magnetic anisotropy [17,18]. In this way, M and I will be parallel to each other. Figure 3 insets show hysteresis loops of the sample taken at the angles of 0°and 90°. Easy and hard axes of the sample are at $\varphi = 0°$(blue) and $\varphi = 90°$(red), respectively.

In magnetoresistive experiments, two types of measurements were performed to compare the relationship between the resistance and applied magnetic field. The first is the dependence of AMR and PHE voltages on the magnetic field while the sample is at a fixed angle. The second is the dependence of the AMR and PHE voltages on the angle at the fixed magnetic field.

Figure 4 shows the dependence of AMR on the magnetic field at specified angles. First, while the applied external magnetic field was parallel to the current, the voltage value was simultaneously recorded. Resistance measurement of the sample as a function of the field reveals typical AMR behavior as shown in Figure 4a. Then,

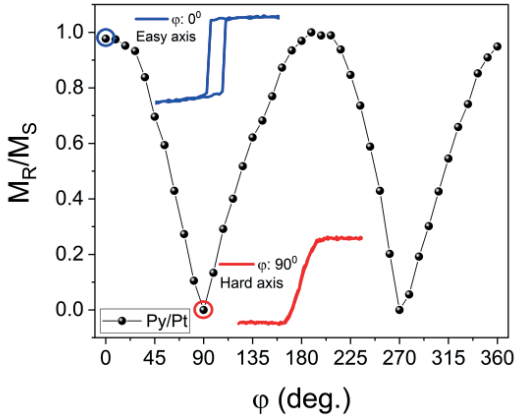

Figure 3. Angle-dependent behavior of the normalized remanent magnetization (M_R/M_S) of the magnetoresistive Py/Pt sensor. Easy and hard axes of the sample are at $\varphi = 0°$(blue) and $\varphi = 90°$(red), respectively.

the sample was rotated by 45° at in-plane geometry. Thus, the φ_H angle between the external magnetic field and the current was 45°. However, in this angle, the sample exhibited unusual AMR behavior as in Figure 4b. At the high magnetic fields which are required to saturate the sample, the Py magnetic moments are aligned along the external magnetic field direction as shown in Region 1 on the inset in Figure 4b. While the H_{ext} was reduced beyond Region 2, the resistance was increased. However, when the magnetic field was further reduced, the resistance of the sample was abruptly decreased due to a greater scattering for a transport electron as shown in Region 3 on the inset in Figure 4b. When the external magnetic field was zero, the R_{AMR} was maximum. At this point, the magnetic moments of the sample begin to rotate. Then, while the magnetic field was increased in a negative direction, the resistance of the sample was again decreased throughout region 4 on the inset in Figure 4b. Further increase in the applied external magnetic field caused a typical decrease in R_{AMR} as shown in Region 5. In the negative high magnetic fields, the magnetic moments of the sample were rotated in the opposite direction to the external magnetic field direction as shown in Region 6 on the inset in Figure 4b. However, in case the applied external magnetic field was perpendicular to the current, unusual peaks in Regions 3 and 4 on the inset in Figure 4b almost vanished as shown in Figure 4c.

To further investigate the unusual peaks in the AMR measurements, PHE measurements were performed at various angles. Then AMR and PHE measurements were compared in terms of magnitude. During the PHE measurements, a constant current of 50 µA was passed through between 2 and 7 terminals in the long direction of the Hall bar. Then, PHE voltage was recorded by using nanovoltmeter between 1 and 3 terminals (V_{1-3}) while the in-plane magnetic field was swept. Figure 5 shows the dependence of PHE voltage on the magnetic field at specified angles. First, the applied external magnetic field was kept parallel to the current and perpendicular to voltage as shown in Figure 5a. The resistance of the sample as a function of the magnetic field exhibited typical PHE behavior. Then, the sample was rotated by 45°at in-plane geometry. The φ_H angle between the external magnetic field and the current was 45°while R_{PHE} measurement of the sample was carried out as shown in Figure 5b. Figures 5a and 5b were compared in terms of resistance and it was observed that the resistance increased significantly while the sample was rotated by 45°. Later, the applied external magnetic field was kept perpendicular to the current parallel to the voltage as shown in Figure 5c. Unlike previous PHE signals in Figures 5a and 5b, the nontypical PHE signal was observed in Figure. 5c.

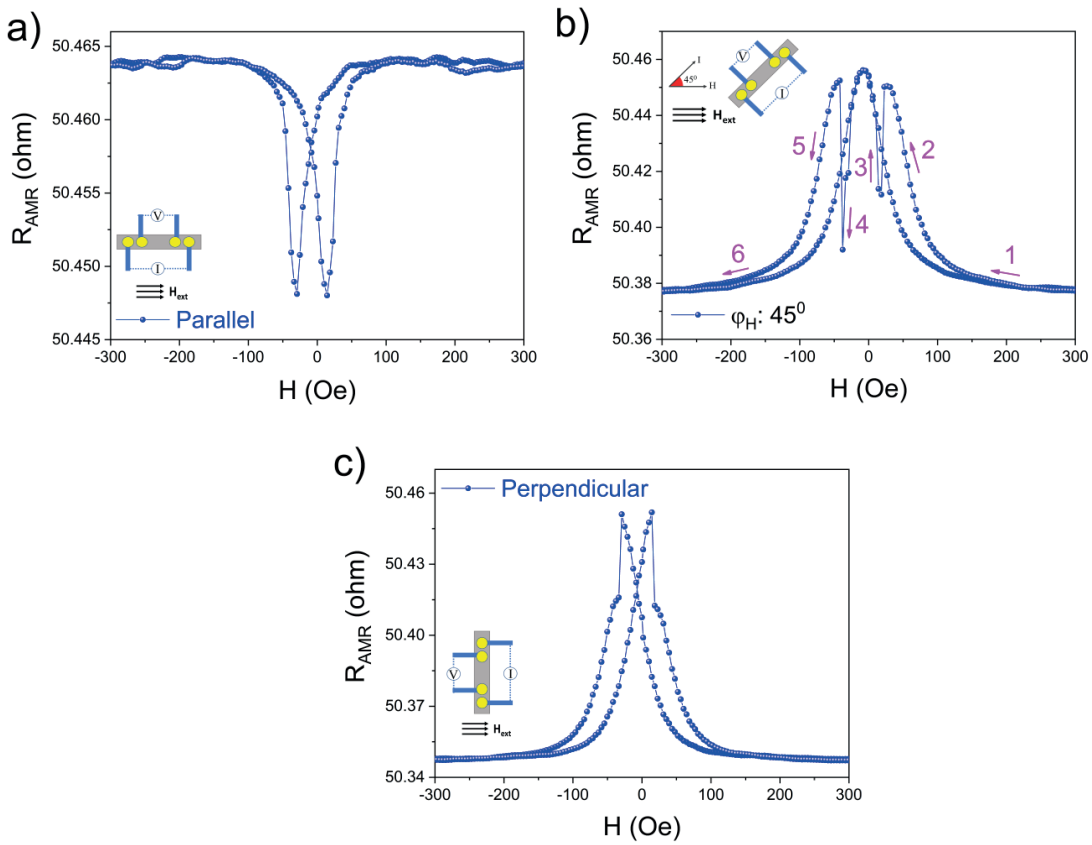

Figure 4. AMR characterizations of the sample. a) applied external magnetic field is parallel to the current, b) the φ_H angle between the external magnetic field and current is 45°, and c) applied external magnetic field is perpendicular to the current.

Figures 4b and 5b were compared to investigate the unusual peaks in the AMR signal and the unusual valleys of the PHE signal as shown in Figure 6. It was seen that unusual peaks in the AMR signal and valleys of the PHE signal were overlapped. In addition to this, the amplitude of unusual peaks in the AMR signal was affected due to the PHE signal at different angles.

The angle-dependent AMR and PHE measurements at the in-plane magnetic field of constant magnitude of 300 Oe were performed to find the maximum amplitude of unusual peaks in the AMR signal. Figure 7 shows the angle-dependent AMR and PHE measurements. The AMR and PHE resistance values were normalized to the resistance of the sample measured at magnetic saturation. Both AMR and PHE curves are matched very well with theoretical predictions. More importantly, there are a few intersection points at certain angles. The intersections of R_{AMR} and R_{PHE} are shown in pink circles as shown in Figure 7. At these intersection points, AMR and PHE curves had strongly affected each other.

4. Conclusion

The NiFe/ Pt magnetoresistive sensor was prepared to compare PHE and AMR effects by using standard microlithography and sputter deposition techniques. Then, the L-MOKE measurements were performed for the sample at room temperature. The L-MOKE measurements show that the sample has an in-plane uniaxial

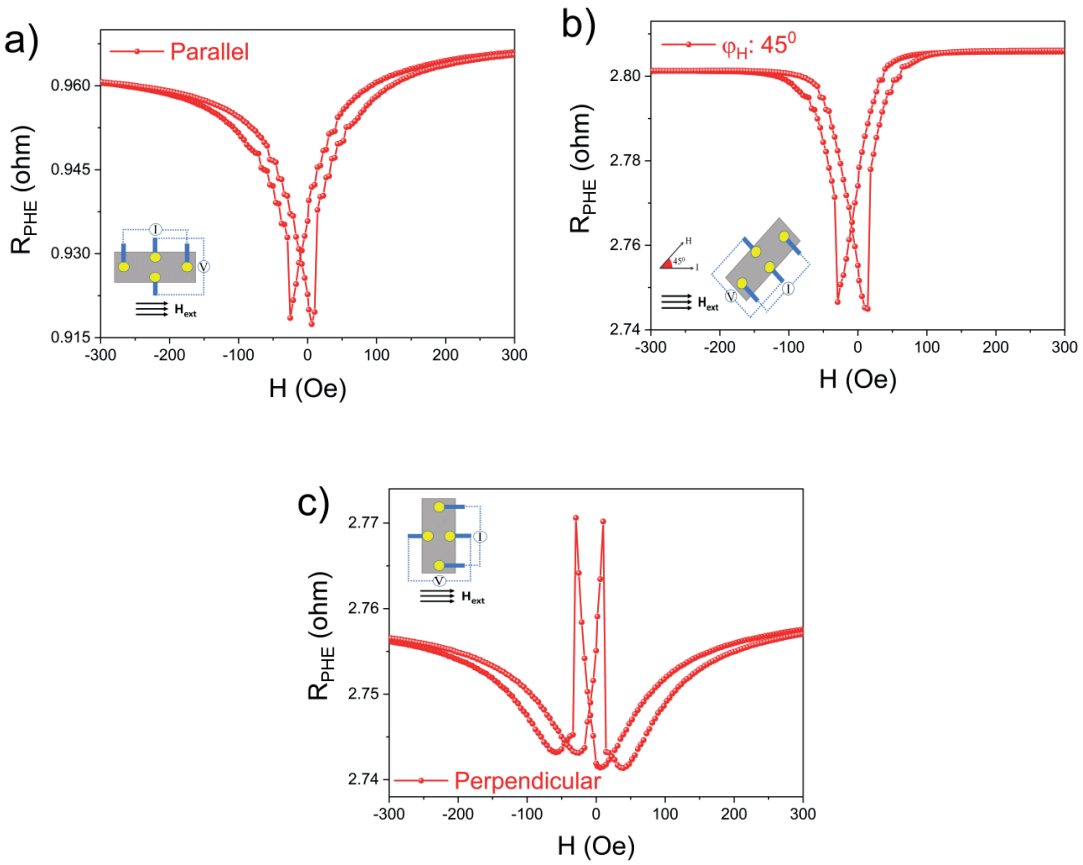

Figure 5. PHE characterizations of the sample. a) applied external magnetic field is parallel to the current, b) the φ_H angle between the external magnetic field and current is 45°, and c) applied external magnetic field is perpendicular to the current.

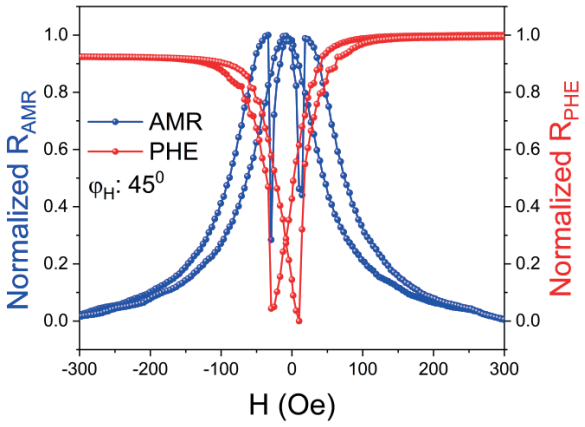

Figure 6. Direct comparison of the AMR (blue) and PHE (red) curves of the magnetoresistive Py/ Pt sensor at $\varphi = 45°$.

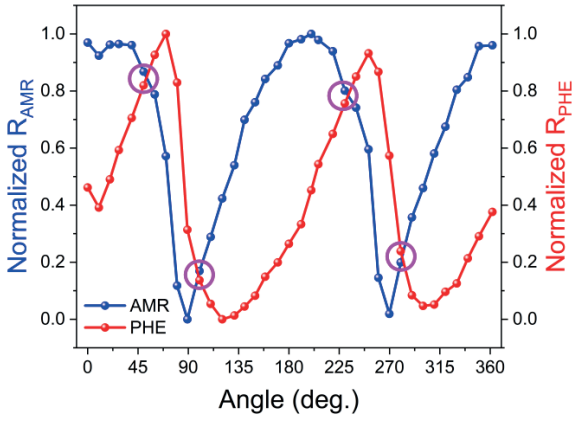

Figure 7. Normalized R_{AMR} (blue) and R_{PHE} (red) curves are plotted as a function of the orientation of the applied field. The R_{AMR} and R_{PHE} curves intersect at specified angles shown in pink circles.

magnetic anisotropy. Also, the easy axis of magnetization extends along the Hall bar of the sample due to the growth-induced magnetic anisotropy. Magneto-transport measurements were carried out along with magnetic measurements. It was observed that AMR and PHE curves have unusual peaks and valleys at the same angle, respectively. In order to determine these angles, the angle-dependent magneto-transport measurements were taken. The angle-dependent AMR and PHE measurements at the in-plane magnetic field of constant magnitude are compatible with theoretical predictions. The measurements also showed that AMR and PHE curves intersect at certain angles. At these angles, the magnetic-field-dependent measurements of AMR and PHE at specified angles showed unusual peaks and valleys. It is proof that AMR and PHE curves had strongly affected each other at certain angles.

References

[1] Freitas PP, Ferreira R, Cardoso S, Cardoso F. Magnetoresistive sensors. Journal of Physics: Condensed Matter 2007; 19 (16): 165221. doi: 10.1088/0953-8984/19/16/165221

[2] Hauser H, Stangl G, Hochreiter J. High-performance magnetoresistive sensors. Sensors and Actuators A: Physical 2000; 81 (1): 27-31. doi: 10.1016/S0924-4247(99)00165-X

[3] Sreevidya PV, Khan J, Barshilia HC, Ananda C, MChowdhury P. Development of two axes magnetometer for navigation applications. Journal of Magnetism and Magnetic Materials 2018; 448 298-302. doi: 10.1016/j.jmmm.2017.08.064

[4] Guo Y, Deng Y, Wang SX. Multilayer anisotropic magnetoresistive angle sensor. Sensors and Actuators A: Physical 2017; 263 159-165. doi: 10.1016/j.sna.2017.06.001

[5] Guo Y, Ouyang Y, Sato N, Ooi CC, Wang SX. Exchange-Biased Anisotropic Magnetoresistive Field Sensor. IEEE Sensors Journal 2017; 17 (11): 3309-3315. doi: 10.1109/JSEN.2017.2695238

[6] Albisetti E, Petti D, Cantoni M, Damin F, Torti A et al. Conditions for efficient on-chip magnetic bead detection via magnetoresistive sensors. Biosensors and Bioelectronics 2013; 47 213-217. doi: 10.1016/j.bios.2013.03.016

[7] Graham DL, Ferreira HA, Freitas PP. Magnetoresistive-based biosensors and biochips. Trends in Biotechnology 2004; 22 (9): 455-462. doi: 10.1016/j.tibtech.2004.06.006

[8] Kim K, Hall DA, Yao C, Lee J-R, Ooi CC et al. Magnetoresistive biosensors with on-chip pulsed excitation and magnetic correlated double sampling. Scientific Reports 2018; 8 (1): 16493. doi: 10.1038/s41598-018-34720-0

[9] Montaigne F, Schuhl A, Van Dau FN, Encinas A. Development of magnetoresistive sensors based on planar Hall effect for applications to microcompass. Sensors and Actuators A: Physical 2000; 81 (1): 324-327. doi: 10.1016/S0924-4247(99)00102-8

[10] Wang Z, Wang X, Li M, Gao Y, Hu Z et al. Highly Sensitive Flexible Magnetic Sensor Based on Anisotropic Magnetoresistance Effect. Advanced Materials 2016; 28 (42): 9370-9377. doi: 10.1002/adma.201602910

[11] Özer B, Pişkin H, Akdoğan N. Shapeable Planar Hall Sensor with a Stable Sensitivity Under Concave and Convex Bending. IEEE Sensors Journal 2019; 19 (14): 5493-5498. doi: 10.1109/JSEN.2019.2907616

[12] Díaz-Michelena M, Cobos PAroca C. Lock-in amplifiers for AMR sensors. Sensors and Actuators A: Physical 2015; 222 (Supplement C): 149-159. doi: 10.1016/j.sna.2014.11.005

[13] McGuire T, Potter R. Anisotropic magnetoresistance in ferromagnetic 3d alloys. IEEE Transactions on Magnetics 1975; 11 (4): 1018-1038. doi: 10.1109/TMAG.1975.1058782

[14] Nguyen Van Dau F, Schuhl A, Childress JR, Sussiau M. Magnetic sensors for nanotesla detection using planar Hall effect. Sensors and Actuators A: Physical 1996; 53 (1): 256-260. doi: 10.1016/0924-4247(96)01152-1

[15] Lu ZQ, Pan G, Lai WY. Planar Hall effect in NiFe/NiMn bilayers. Journal of Applied Physics 2001; 90 (3): 1414-1418. doi: 10.1063/1.1380993

[16] Pişkin H, Akdoğan N. Interface-induced enhancement of sensitivity in NiFe/Pt/IrMn-based planar hall sensors with nanoTesla resolution. Sensors and Actuators A: Physical 2019; 292 24-29. doi: 10.1016/j.sna.2019.04.003

[17] Knorr TG, Hoffman RW. Dependence of geometric magnetic anisotropy in thin iron films. Physical Review 1959; 113 (4): 1039-1046. doi: 10.1103/PhysRev.113.1039

[18] Özdemir M, Aktas B, Öner Y, Sato TAndo T. Anomalous anisotropy of re-entrant film. Journal of Physics: Condensed Matter 1997; 9 (30): 6433-6445. doi: 10.1088/0953-8984/9/30/012